RESEARCH ARTICLE

NANO · MICRO small
www.small-journal.com

Securing LYTAC with Logic-Identification System for Cancer Cell-Selective Membrane Protein Degradation

*Yanyun Fang, Yue Zhang, Shiyi Bi, Bo Peng, Caixia Wang, Huangxian Ju, and Ying Liu**

Lysosome-targeting chimera (LYTAC) links proteins of interest (POIs) with lysosome-targeting receptors (LTRs) to achieve membrane protein degradation, which is becoming a promising therapeutic modality. However, cancer cell-selective membrane protein degradation remains a big challenge considering expressions of POIs in both cancer cells and normal cells, as well as broad tissue distribution of LTRs. Here a logic-identification system is designed, termed Logic-TAC, based on cell membrane-guided DNA calculations to secure LYTAC selectively for cancer cells. Logic-TAC is designed as a duplex DNA structure, with both POI and LTR recognition regions sealed to avoid systematic toxicity during administration. MCF-7 and MCF-10A are chosen as sample cancer cell and normal cell respectively. As input 1 for logic-identification, membrane proteins EpCAM, which is highly expressed by MCF-7 but barely by MCF-10A, reacts with Logic-TAC to expose POI recognition region. As input 2 for logic-identification, Logic-TAC binds to POI, membrane protein MUC1, to expose LTR recognition region. As output, MUC1 is connected to LTR and degraded *via* lysosome pathway selectively for cancer cell MCF-7 with little side effect on normal cell MCF-10A. The logic-identification system also demonstrated satisfactory *in vivo* therapeutic results, indicating its promising potential in precise targeted therapy.

1. Introduction

Membrane proteins account for one-third of all proteins expressed by the genomes of most organisms and take part in a wide range of important biochemical and physiological processes,[1–4] which makes them critical targets for a variety of diseases.[5–7] *Via* directly connecting membrane proteins of interest (POIs) to lysosome-targeting receptors (LTRs), synthesized lysosome-targeting chimeras (LYTACs) bring membrane POIs to lysosomes for degradation,[8–10] and has achieved encouraging outcomes in therapy.[11–13]

However, considering target membrane POI is also expressed by normal cells besides objective cancer cells, only endowing LYTACs with POIs recognition specificity is not enough.[14] Failure to control LYTAC binding order to POI and LTR impairs POI degradation efficiency and would bring off-target effect. Take mucins for example, besides widely expressed by most carcinomas,[15] it also expressed on normal epithelial and endothelial cells by acting as a physical barrier to defend against physical insults and pathogens.[16] The systemic administration of LYTAC molecules and their diffused distribution would unavoidably degrade POI for non-cancerous cells and lead to corresponding systemic toxicity.[17–20] Therefore, developing cancer cell-selective membrane POIs degradation strategy while avoiding systematic toxicity elsewhere is in urgent need.

Through modifying TACs with cancer cell-specific internalization molecules, such as folate,[19] aptamer AS1411[21], or cleavable/transformable molecules responsive to cancer cell internal environment (GSH[22]/protease[23–25]), controlled degradation strategies have been developed for intracellular POIs with PROTACs. However, the connections of membrane POIs and LTRs occur at cell membrane for LYTAC strategies. In addition, LTRs such as cation-independent mannose-6-phosphate receptor (CI-M6PR, also called IGFIIR) have broad tissue distribution and couldn't contribute to the cancer cell-selective internalization of POIs.[26,27] These factors all limited the application of controllable targeted protein degradation (TPD) strategies only for PROTACs and hardly extended to LYTACs with membrane POIs.

Recently cancer cell-associated mucin degradation has been successfully achieved through designing selective protease,[28] which relies on sophisticated protein engineering procedures and requires individual protease design when applied for different membrane POIs. Here we develop a logic-identification system endowed LYTAC, termed "Logic-TAC", with the capability of "SEquential reCOgnition and REconfiguration" (SECORE) for cancer cell-selective membrane protein degradation with

Y. Fang, S. Bi, B. Peng, C. Wang, H. Ju, Y. Liu
State Key Laboratory of Analytical Chemistry for Life Science
School of Chemistry and Chemical Engineering
Nanjing University
Nanjing 210023, China
E-mail: yingliu@nju.edu.cn

Y. Zhang
School of Pharmacy
Nanjing University of Chinese Medicine
Nanjing 210023, China

Y. Liu
Chemistry and Biomedicine Innovation Center
Nanjing University
Nanjing 210023, China

The ORCID identification number(s) for the author(s) of this article can be found under https://doi.org/10.1002/smll.202310039

DOI: 10.1002/smll.202310039

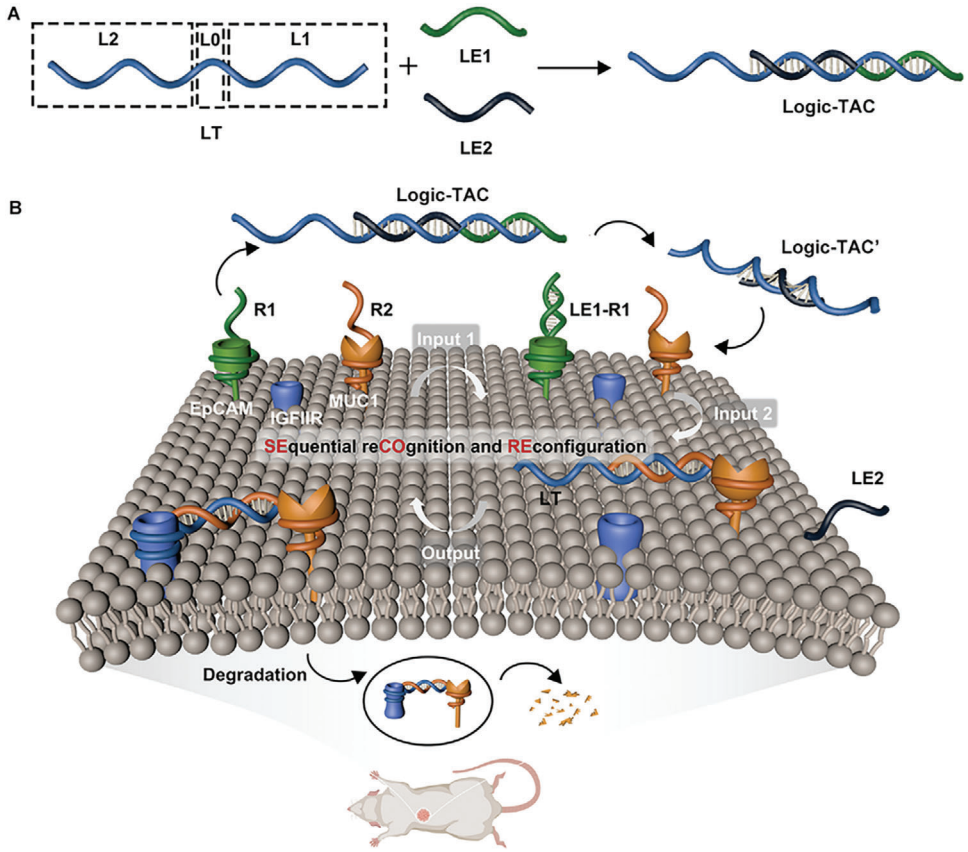

Scheme 1. Cancer cell-selective membrane protein degradation. A) Schematic illustration of Logic-TAC synthesis. B) The scheme of cancer cell-selective MUC1 degradation *via* SECORE strategy.

little systematic toxicity. MCF-7/MCF-10A are chosen as sample cancer cell/normal cell respectively. Mucin 1 (MUC1) is chosen as sample POI,[29,30] and transmembrane protein epithelial cell adhesion molecule (EpCAM) that highly expressed by MCF-7 and barely expressed by MCF-10A is chosen as cancer cell indicator protein.[31] LYTAC molecule LT consists of L1 for POI MUC1 ligation, L0 linker, and L2 for LTR IGFIIR ligation.[32] LT self-assembles with leaving DNA strand LE1 and LE2 to obtain Logic-TAC as a duplex DNA structure. LE1 and LE2 provide secure sealing of L1 and L2 respectively, therefore Logic-TAC remains inactive in systemic circulation with little toxicity to normal cells/tissues (**Scheme** 1A). SECORE strategy is performed selectively for cancer cell MCF-7 *via* a membrane-guided DNA logic calculation. DNA strands R1 and R2 are pre-bound to EpCAM and MUC1 respectively on cell membrane. To perform input 1 of DNA logic calculation, R1 reacts with Logic-TAC *via* toehold-mediated strand displacement reaction, which forms LE1-R1 duplex on EpCAM and exposes L1 in as-obtained Logic-TAC' for MUC1 ligation (Scheme 1B, Input 1). To perform input 2 of DNA logic calculation, R2 hybridizes with the exposed L1 region *via* toehold-mediated strand displacement reaction, which drops LE2 to obtain LT with exposed L2 for IGFIIR ligation, and anchors LT to MUC1 (Scheme 1B, Input 2). As the output of DNA logic calculation, MUC1 is connected to IGFIIR (Scheme 1B, Output) and degraded *via* lysosome pathway (Scheme 1B, Degradation). As for normal cell MCF-10A, Logic-TAC could not ligate to MUC1 in the absence of indicator protein EpCAM and correspondingly invalided input 1 calculation, which secures POI degradation selectively for cancer cells and avoids nonspecific toxicity to normal cells/undesired tissues that also expressed POIs. In addition, SECORE strategy guarantees only "activated" LYTAC molecule that bound to MUC1 can ligate IGFIIR, which prevents the invalid endocytosis of "unloaded" LYTAC molecules and enhances POI degradation efficiency. Furthermore, the SECORE strategy could be expanded to other membrane proteins based on the modular design of the input DNA strand. Therefore, it would have a promising contribution to precisely targeted therapy.

2. Results and Discussion

2.1. Synthesis of P-LYTAC and its Anchoring to MCF-7 Cells

Sequential recognition and ligation to POI and LTR is the key for the logic programming of LYTAC molecule. Considering IGFIIR indiscriminately internalizes LYTAC molecule no matter it ligates with POI or not, the binding order of LYTAC to POI and IGFIIR affects POI degradation efficiency. As a proof of concept, photo irradiation was used to regulate the sequential ligation of LYTAC molecule to POI MUC1 and IGFIIR. Photo-responsive LYTAC (P-LYTAC) was correspondingly synthesized by hybridizing LYTAC strand (LY, 79 nt) and photo cleavable block strand (LB, 38 nt). LY contained IGFIIR ligation region (L2, 40 nt) and MUC1 ligation

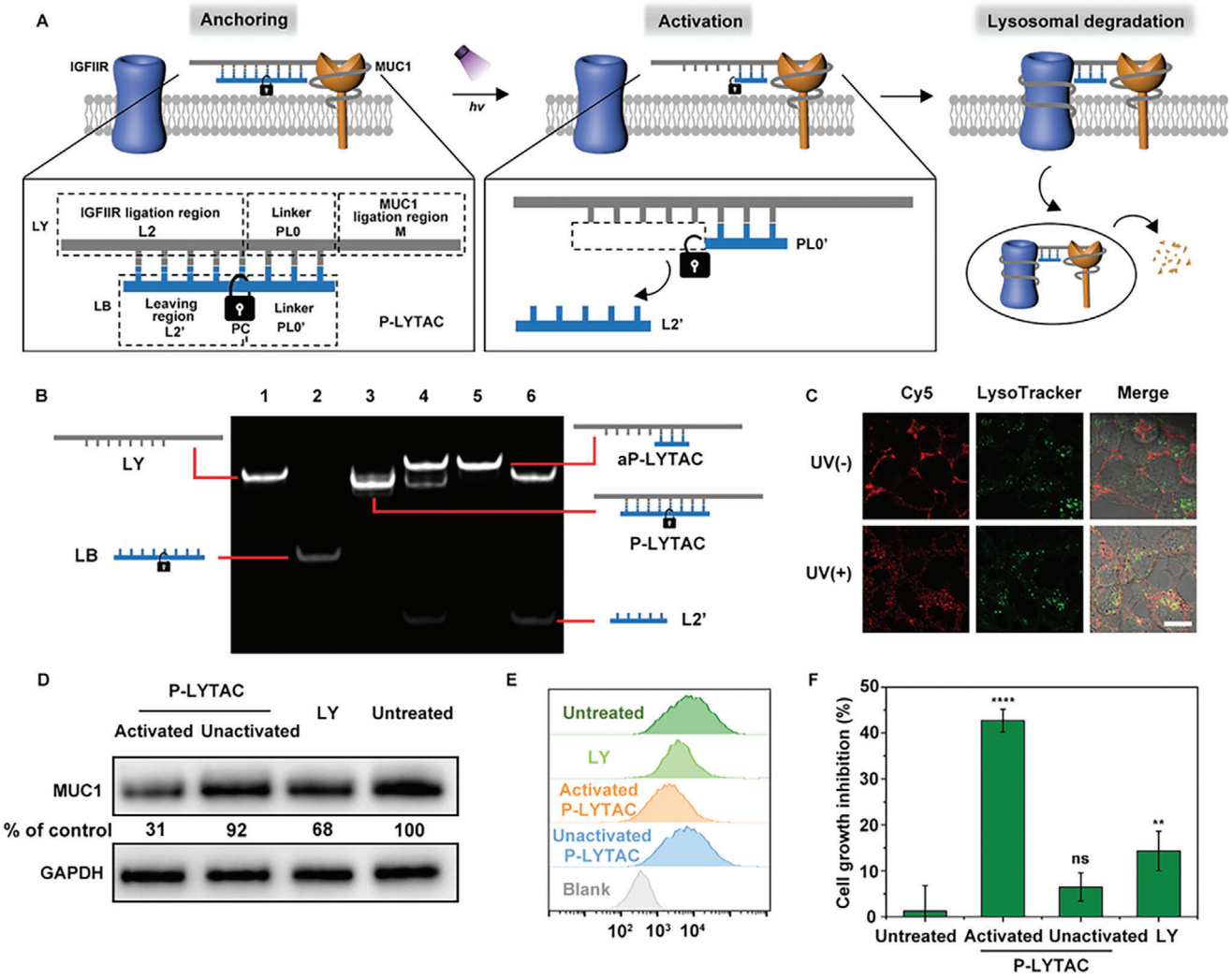

Figure 1. Synthesis and operation of P-LYTAC for controlled protein degradation. A) Schematic illustration of P-LYTAC structure and MUC1 degradation upon photo activation. B) PAGE verification for photo-activation of P-LYTAC. Lane 1–6: LY, LB, P-LYTAC, P-LYTAC with UV irradiation, mixture of LY+PL0', and mixture of LY+L2'. C) Confocal microscopic images of P-LYTAC$_{Cy5}$ treated MCF-7 cells with and without UV irradiation, and colocalized with LysoTracker Green. The scale bar is 15 μm. D) Immunoblot analysis, E) flow cytometry analysis of MUC1 expressions, and F) quantification of cell growth inhibition of untreated MCF-7 cells, and MCF-7 cells treated respectively with LY, UV irradiation activated P-LYTAC (Activated P-LYTAC) and P-LYTAC without UV irradiation (Unactivated P-LYTAC). The level of MUC1 expression for untreated MCF-7 was set as the control in (D). The data error bars in (F) indicate means ± S.D. (n = 3). $^{**}p < 0.01$ and $^{****}p < 0.0001$ with two-tailed Student's t-test.

region (M, 25 nt), which were connected by a linker (PL0, 14 nt). LB contained linker (PL0', 14 nt) and leaving region (L2', 24 nt), which were connected through the o-nitrobenzyl derived photocleavable linker molecule (PC) (Figure S1, Supporting Information). PL0' was completely complementary to PL0, while L2' was partially complementary to L2 with one mismatched base spaced in every three complementary bases. Hybridization of LB to LY blocked IGFIIR recognition while MUC1 recognition was not affected. Therefore, the as-obtained P-LYTAC only anchored on cell membrane *via* binding to MUC1 (**Figure** 1A, Anchoring), which avoided invalid internalization of "unloaded" LYTAC molecule through IGFIIR ligation.

The successful construction of P-LYTAC was confirmed by PAGE analysis, which showed a new band upon the mixture of LY and LB (Figure 1B, Lane 1, 2, 3). To visualize the anchoring of P-LYTAC on cell membrane, Cy5-labeled P-LYTAC (P-LYTAC$_{Cy5}$) was prepared *via* hybridizing LY$_{Cy5}$ and LB (Figure S2A, Supporting Information), and incubated with MCF-7 cells that express MUC1. It demonstrated clear Cy5 fluorescence on cell membrane under confocal laser scanning microscopy (CLSM) (Figure S2B, P-LYTAC$_{Cy5}$, Supporting Information). Membrane Cy5 fluorescence increased with the concentration of P-LYTAC$_{Cy5}$, and saturated at 1 μM (Figure S3, Supporting Information). Cy5-labeled MUC1 aptamer (A-MUC1$_{Cy5}$) was also incubated with MCF-7 cells, which demonstrated similar intensity of Cy5 fluorescence from cell membrane (Figure S2B, A-MUC1$_{Cy5}$, Supporting Information). Flow cytometry demonstrated similar results (Figure S2C, P-LYTAC$_{Cy5}$, A-MUC1$_{Cy5}$, Supporting Information), confirmed the efficient anchoring of P-LYTAC$_{Cy5}$ on cell membrane. Nonspecific P-LYTAC$_{Cy5}$ (ns P-LYTAC$_{Cy5}$) with scrambled

sequence in M region that doesn't recognize MUC1 showed membrane fluorescence neither from CLSM (Figure S2B, ns P-LYTAC$_{Cy5}$, Supporting Information) nor flow cytometry (Figure S2C, ns P-LYTAC$_{Cy5}$, Supporting Information), indicating good specificity of P-LYTAC anchoring.

2.2. P-LYTAC Ligation to IGFIIR and MUC1 Degradation

L2' couldn't form stable duplex structure with LY, and showed two separate bands on PAGE upon mixture (Figure 1B, lane 6). Therefore, UV irradiation cleaved PC, which activated P-LYTAC by detaching L2' and exposing IGFIIR ligation region L2 (Figure 1A, Activation). The activated P-LYTAC was then ligated to IGFIIR and correspondingly degraded MUC1 (Figure 1A, Lysosomal degradation). Photo irradiation of P-LYTAC generated two new bands on PAGE at the corresponding positions of L2' and aP-LYTAC (LY hybridizing with PL0') (Figure 1B, lane 4). To confirm photo activation of P-LYTAC on cell membrane, dual-labeling P-LYTAC (P-LYTAC$_{FAM/Cy5}$) was prepared by hybridizing Cy5 labeled LY (LY$_{Cy5}$) with FAM labeled LB (LB$_{FAM}$) (Figure S4A, Supporting Information). P-LYTAC$_{FAM/Cy5}$ incubated MCF-7 cell demonstrated strong Cy5 and FAM fluorescence on cell membrane in the absence of photo irradiation (Figure S4, UV(−), Supporting Information), while FAM fluorescence was significantly decreased from cell membrane in the presence of photo-irradiation due to the cleavage of L2' (Figure S4, UV(+), Supporting Information). To further verify the internalization of activated P-LYTAC, P-LYTAC$_{Cy5}$ anchored MCF-7 cells were continuously imaged for 60 min after photo irradiation, and it demonstrated clear intracellular distribution of Cy5 fluorescence that completely deviated from DiO fluorescence on cell membrane (Figure S5, UV(+), Supporting Information). On the contrary, Cy5 fluorescence mainly remained on cell membrane and well overlapped with DiO fluorescence for P-LYTAC$_{Cy5}$ anchored MCF-7 cells in the absence of photo-irradiation due to the good sealing of IGFIIR ligation region (Figure S5, UV(−), Supporting Information).

To trace the subsequent transfer of MUC1 to lysosome, Cy5 fluorescence for P-LYTAC$_{Cy5}$ treated MUC1 cells was further colocalized with lysosomal dye LysoTracker Green. Cy5 fluorescence was mainly observed intracellularly and well overlapped with LysoTracker fluorescence for photo irradiated group (Figure 1C, UV(+)). On the contrary, Cy5 fluorescence was mainly observed on cell membrane in the absence of photo irradiation (Figure 1C, UV(−)). Pearson's correlation coefficient for Cy5 fluorescence and LysoTracker Green fluorescence increased from 0.04 to 0.51 after photo-irradiation. These results confirmed the efficient endocytosis of photo-activated P-LYTAC *via* lysosome pathway. The administration dosage and incubation time for P-LYTAC were optimized, and 1 μM of P-LYTAC with 24-h incubation was chosen as the experiment condition (Figure S6, Supporting Information).

Immunoblot was further performed to evaluate MUC1 degradation efficiency. Photo-activated P-LYTAC was incubated with MCF-7 cells and demonstrated the most effective suppression with only 31% of MUC1 expression (Figure 1D, Activated P-LYTAC). On the contrary, MUC1 expression level was barely suppressed for MCF-7 cells that incubated with unactivated P-LYTAC (Figure 1D, Unactivated P-LYTAC) compared with untreated MCF-7 cells (Figure 1D, Untreated). It is noteworthy that LYTAC molecule LY demonstrated lower MUC1 degradation efficiency with MUC1 expression of 68% compared with photo-activated P-LYTAC (Figure 1D, LY). Considering IGFIIR ligation region L2 was unsealed in LY, the internalization of LY was irrelevant to MUC1 ligation process. It resulted in invalid endocytosis of "unloaded LY" that didn't bind with MUC1, which impaired MUC1 degradation efficiency compared with P-LYTAC guided degradation. MUC1 expression levels were also confirmed with the flow cytometry analysis by incubating with A-MUC1$_{Cy5}$ to indicate the undegraded MUC1 remained on cell membrane (Figure 1E). It demonstrated similar tendency as immunoblot results. Photo-activated P-LYTAC group showed obvious decrease of Cy5 fluorescence on cell membrane (Figure 1E, Activated P-LYTAC), while LY-treated MCF-7 cells demonstrated limited decrease of Cy5 fluorescence (Figure 1E, LY). P-LYTAC in the absence of photo irradiation (Figure 1E, Unactivated P-LYTAC) barely decreased membrane Cy5 fluorescence compared with untreated MCF-7 cells (Figure 1E, Untreated).

The contribution of MUC1 degradation to the inhibition of cell growth was evaluated by measuring cell viability. P-LYTAC incubated MCF-7 cell showed 42.7% of cell growth inhibition with photo-irradiation activation (Figure 1F, Activated P-LYTAC) and 5.5% of cell growth inhibition without photo-irradiation activation (Figure 1F, Unactivated P-LYTAC). LY incubated MCF-7 cells only showed 14.3% of cell growth inhibition (Figure 1F, LY). These results indicated programming the ligation order of LYTAC molecule to POI and IGFIIR could effectively enhance POI degradation efficiency.

2.3. Synthesis of Logic-TAC and *In Vitro* Verification of SECORE Strategy

To endow sequential ligation and cancer cell selectivity to the classic LYTAC, SECORE strategy was designed which relied on cell membrane-guided DNA calculation to activate LYTAC molecule. Logic-TAC consisted of 63 nt LYTAC strands (LT), 24 nt leaving strand (LE1), and 19 nt leaving strand (LE2). LT consisted of 40 nt LTR IGFIIR ligation region (L2) that directly binds to IGFIIR, a 3 nt linker strand L0, and 20 nt MUC1 ligation region (L1) that contained 12 nt L1-Y and 8 nt L1-G. LE2 had the complementary sequence of L0 and 16 nt of L2 counting from 5' terminus with alternate one and three mismatched base spaced in every four complementary bases, while LE1 was completely complementary to L1 with 4 nt toehold exposed (**Figure 2A**). The effective sealing from LE2 and LE1 blocked ligation of LT to IGFIIR and MUC1 respectively, therefore protecting Logic-TAC from nonspecific activation or invalid consumption in systematic circulation. The successful synthesis of Logic-TAC was confirmed *via* PAGE analysis, which generated a new band with lower mobility upon the mixture of LT, LE1, and LE2 (Figure S7A, Supporting Information).

SECORE strategy was performed by Logic-TAC sequentially reacting with EpCAM and MUC1. R1 contained 48 nt EpCAM recognition aptamer (A-EpCAM) and 24 nt reaction region (c-LE1) that had complementary sequence to LE1. R2 contained 25 nt MUC1 recognition aptamer (A-MUC1) and 15 nt reaction region (c-L1-Y-0) that had complementary sequence to

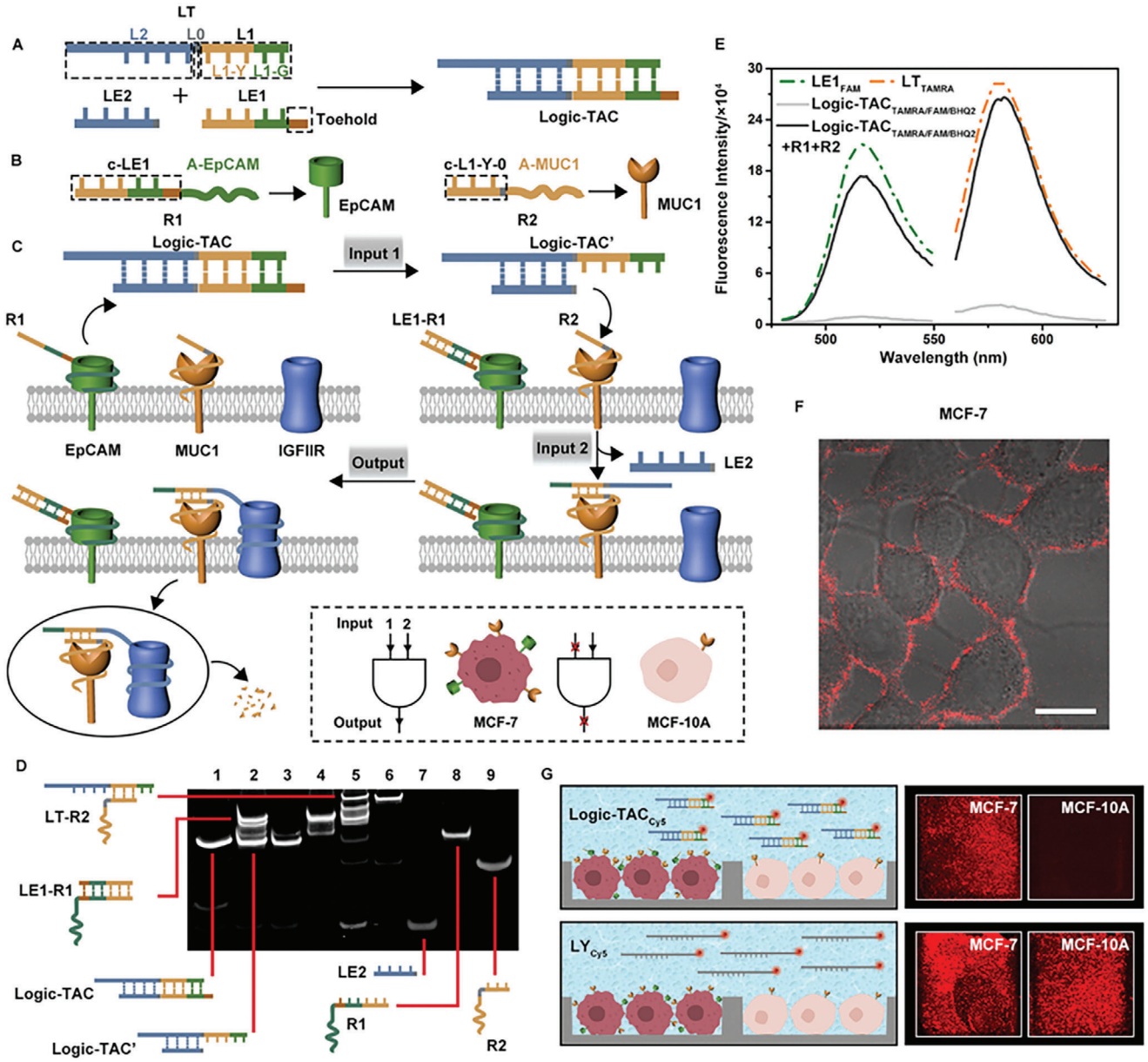

Figure 2. Synthesis and operation of Logic-TAC for cancer cell-selective protein degradation. A) Schematic illustration of Logic-TAC. B) Schematic illustrations of R1, R2, and corresponding ligation to EpCAM, MUC1. C) Schematic illustrations of EpCAM/MUC1 guided DNA logical computation on cell membrane. D) PAGE analysis for Logic-TAC logic computation with R1 and R2. Lane 1–9: Logic-TAC, mixture of Logic-TAC+R1, Logic-TAC', LE1-R1 duplex, mixture of Logic-TAC+R1+R2, LT-R2 duplex, LE2, R1, R2. E) Fluorescence spectra of $LE1_{FAM}$, LT_{TAMRA}, $Logic\text{-}TAC_{TAMRA/FAM/BHQ2}$, and mixture of $Logic\text{-}TAC_{TAMRA/FAM/BHQ2}$+R1+R2. F) CLSM image of $Logic\text{-}TAC_{TAMRA}$ incubated with MCF-7 cells that pretreated with R1 and R2. The scale bar is 15 μm. G) Schematic illustration and Cy5 fluorescence in chamber for MCF-7 cells and MCF-10A cells co-cultivation and treated with R1/R2/$Logic\text{-}TAC_{Cy5}$ and LY_{Cy5} respectively.

L1-Y and L0 (Figure 2B). R1 and R2 were pre-anchored to EpCAM and MUC1 on MCF-7 cell respectively, and c-LE1/c-L1-Y-0 were exposed to guide "AND" logic gate DNA calculation at cell membrane. As input 1 for logic gate, Logic-TAC reacted with membrane-anchored R1, which dropped strand LE1 from Logic-TAC to form a duplex structure with R1 (LE1-R1), and exposed L1 region in as-obtained Logic-TAC' (Figure 2C, Input 1). As input 2 for logic gate, Logic-TAC' continuously reacted with membrane-anchored R2, which dropped LE2 to expose L2 in as-obtained LT, as well as anchored LT to MUC1 on cell membrane (Figure 2C, Input 2). As output of DNA logic gate, LT was ligated to IGFIIR to achieve cancer cell MCF-7 selective MUC1 degradation (Figure 2C, Output), while didn't show nonspecific effect to normal cell MCF-10A.

The operation of SECORE strategy was first verified *via* PAGE analysis (Figure 2D). Incubating Logic-TAC with R1 generated LE1-R1 duplex and Logic-TAC'. Incubating Logic-TAC with R1/R2 generated LE2 and LT-R2 duplex. The band appeared in

between LT-R2 and LE1-R1 may come from R1/R2 hybridization considering their partial complementary sequence (Figure 2D, lane 5). Logic-TAC didn't react with R2 in the absence of R1 (Figure S7B, Supporting Information). This result indicated good reaction specificity of SECORE strategy. To further verify the feasibility of SECORE strategy, Logic-TAC$_{TAMRA/FAM/BHQ2}$ was synthesized by hybridizing TAMRA labelled LT (LT$_{TAMRA}$) with BHQ2 labelled LE2 (LE2$_{BHQ2}$) and FAM labelled LE1 (LE1$_{FAM}$) (Figure S8A, Supporting Information). Incubating self-quenched Logic-TAC$_{TAMRA/FAM/BHQ2}$ with R1 generated LE1-R1$_{FAM}$ and Logic-TAC'$_{TAMRA/BHQ2}$, which recovered FAM fluorescence. Continuously incubating Logic-TAC'$_{TAMRA/BHQ2}$ with R2 recovered TAMRA fluorescence due to the release of LE2, and generated LT-R2$_{TAMRA}$ (Figure S8A, Correct calculation, Supporting Information). Therefore, Logic-TAC$_{TAMRA/FAM/BHQ2}$ co-incubating with R1 and R2 showed fluorescence recoveries for both TAMRA and FAM (Figure 2E). On the contrary, SECORE strategy could not proceed in the absence of input 1, therefore incubating Logic-TAC$_{TAMRA/FAM/BHQ2}$ with R2 didn't recover FAM or TAMRA fluorescence (Figure S8A, Incorrect calculation, C, Supporting Information). To verify DNA calculation specificity, mutant R1 (m-R1) and mutant R2 (m-R2) were prepared with mismatched sequence of LE1 and mismatched sequence of L1-Y-0 respectively. Mutant R1/R2 could not perform DNA calculation, therefore couldn't recover TAMRA fluorescence (Figure S9, Supporting Information).

2.4. Operation of Cancer Cell-Selective SECORE Strategy

Logic-TAC$_{TAMRA}$ was prepared with LT$_{TAMRA}$ and incubated with MCF-7 cells and MCF-10A cells respectively. Both cell lines were pretreated with R1 and R2. MCF-7 cells clearly demonstrated TAMRA fluorescence on cell membrane (Figure 2F), while MCF-10A cells barely showed TAMRA fluorescence (Figure S10, Supporting Information), indicating SECORE strategy could not proceed in the absence of input 1 calculation. In addition, MCF-7 cells that pretreated with m-R1 and R2, or R1 and m-R2 didn't show TAMRA fluorescence either (Figure S11, Supporting Information), indicating SECORE strategy could not proceed with calculation error in step 1 or step 2. These results confirmed the cancer cell-selective Logic-TAC activation *via* the operation of DNA logic gate on cell membrane. MCF-7 and MCF-10A cells were further co-cultured in the multicell co-cultivation apparatus to mimic biological environment with the coexistence of cancer cells and normal cells. Logic gate embedded LYTAC molecule Logic-TAC$_{Cy5}$ clearly discriminated cancer cell with normal cell, and only showed Cy5 fluorescence on MCF-7 cells (Figure 2G, Logic-TAC$_{Cy5}$). On the control, regular LYTAC molecule, LY$_{Cy5}$ could anchor to cells from MUC1 ligation or IGFIIR ligation, and showed Cy5 fluorescence both from MCF-7 cells and MCF-10A cells (Figure 2G, LY$_{Cy5}$). These results confirmed the capability of SECORE strategy to selectively recognize cancer cell POI in cell mixture.

Along with the cancer cell-selective ligation of Logic-TAC to IGFIIR, MUC1 was degraded *via* lysosomal pathway. Cy5 labeled R2 (R2$_{Cy5}$) was used as indicator to trace MUC1 during the lysosomal degradation process. Only MCF-7 cells with DNA logic calculation process showed Cy5 fluorescence intracellularly, which co-localized well with LysoTracker fluorescence with Pearson's correlation coefficient of 0.76, confirming the efficient internalization of MUC1 *via* lysosome transport (**Figure** 3A, R1/R2$_{Cy5}$).

The control groups of unsuccessful DNA logic calculation for MCF-7 cells pretreated with m-R1/R2$_{Cy5}$ and R1/m-R2$_{Cy5}$ respectively showed much lower Pearson's correlation coefficients of 0.11, 0.03, and MCF-7 cells pretreated with R2$_{Cy5}$ showed similar Pearson's correlation coefficients of 0.07 (Figure 3A, m-R1/R2$_{Cy5}$, R1/m-R2$_{Cy5}$, R2$_{Cy5}$). The intensity of membrane Cy5 fluorescence was also quantified and compared with whole cell Cy5 fluorescence, which demonstrated the lowest value for R1/R2 pretreated MCF-7 cells, further confirming effective internalization of MUC1 with DNA logic calculation (Figure S12, Supporting Information). The administration dosage and incubation time for Logic-TAC were optimized, and 1 μM of Logic-TAC with 24-h incubation was chosen as the experiment condition (Figure S13, Supporting Information). The precise operation of SECORE strategy on cell membrane for MUC1 degradation was further verified by immunofluorescence staining. Substantial MUC1 decrease was observed for R1/R2 pretreated MCF-7 cells compared with untreated MCF-7 cell and two miscalculated control groups that pretreated with m-R1/R2 and R1/m-R2 respectively (Figure S14, Supporting Information). After staining MUC1 with A-MUC1$_{Cy5}$, its cell- selective degradation was further analyzed *via* flow cytometry. MCF-7 demonstrated obvious MUC1 decrease after Logic-TAC treatment, while MCF-10A showed little change (Figure 3C, Logic-TAC), indicating SECORE strategy could effectively discriminate cancer cells with noncancerous cells for POI degradation. Control Logic-TAC probe (Logic-TAC') was prepared by hybridizing LT with LE2 (Figure 3B, Logic-TAC'). The successful synthesis of Logic-TAC' and corresponding calculation with R1 or R1/R2 was confirmed by PAGE analysis (Figure S15, Supporting Information). Due to the absence of LE1, Logic-TAC' lacks the capability of cancer cell discrimination. Therefore, both MCF-7 cells and MCF-10A cells showed obvious MUC1 decrease (Figure 3C, Logic-TAC').

To evaluate the contribution of SECORE strategy to POI degradation efficiency, control Logic-TAC probe-2 (Logic-TAC'-2) was prepared by hybridizing LY with 34 nt LE1'. LE1' blocked IGFIIR ligation region on LY, and could be released by R1' that pre-anchored on EpCAM, therefore the ligation of Logic-TAC'-2 to IGFIIR was controlled by EpCAM recognition (Figure 3B, Logic-TAC'-2). R1' consisted of A-EpCAM that recognized membrane protein EpCAM and c-LE1' that had complementary sequence as LE1'. The successful synthesis of Logic-TAC'-2 and corresponding calculation with R1' was confirmed *via* PAGE analysis (Figure S16, Supporting Information). With EpCAM participating in DNA calculation, Logic-TAC'-2 well discriminated MCF-7 cells with MCF-10A cells, and demonstrated MUC1 decrease for MCF-7 cells while affecting MCF-10A cells little (Figure 3C, Logic-TAC'-2). However, Logic-TAC'-2 lacks logic order for MUC1 ligation and IGFIIR ligation, thus "invalid" internalization of "unloaded" Logic-TAC'-2 compromised MUC1 degradation efficiency. It showed less efficient MUC1 decrease compared with Logic-TAC treated MCF-7 cells. MUC1 expression levels for MCF-7 cells and MCF-10A cells were also evaluated respectively *via* immunoblot after treating with different LYTAC strategies. Logic-TAC treatment resulted in 27% of MUC1 expression for MCF-7 cells but barely affected MUC1 expression for MCF-10A cells, while Logic-TAC' showed the obvious MUC1

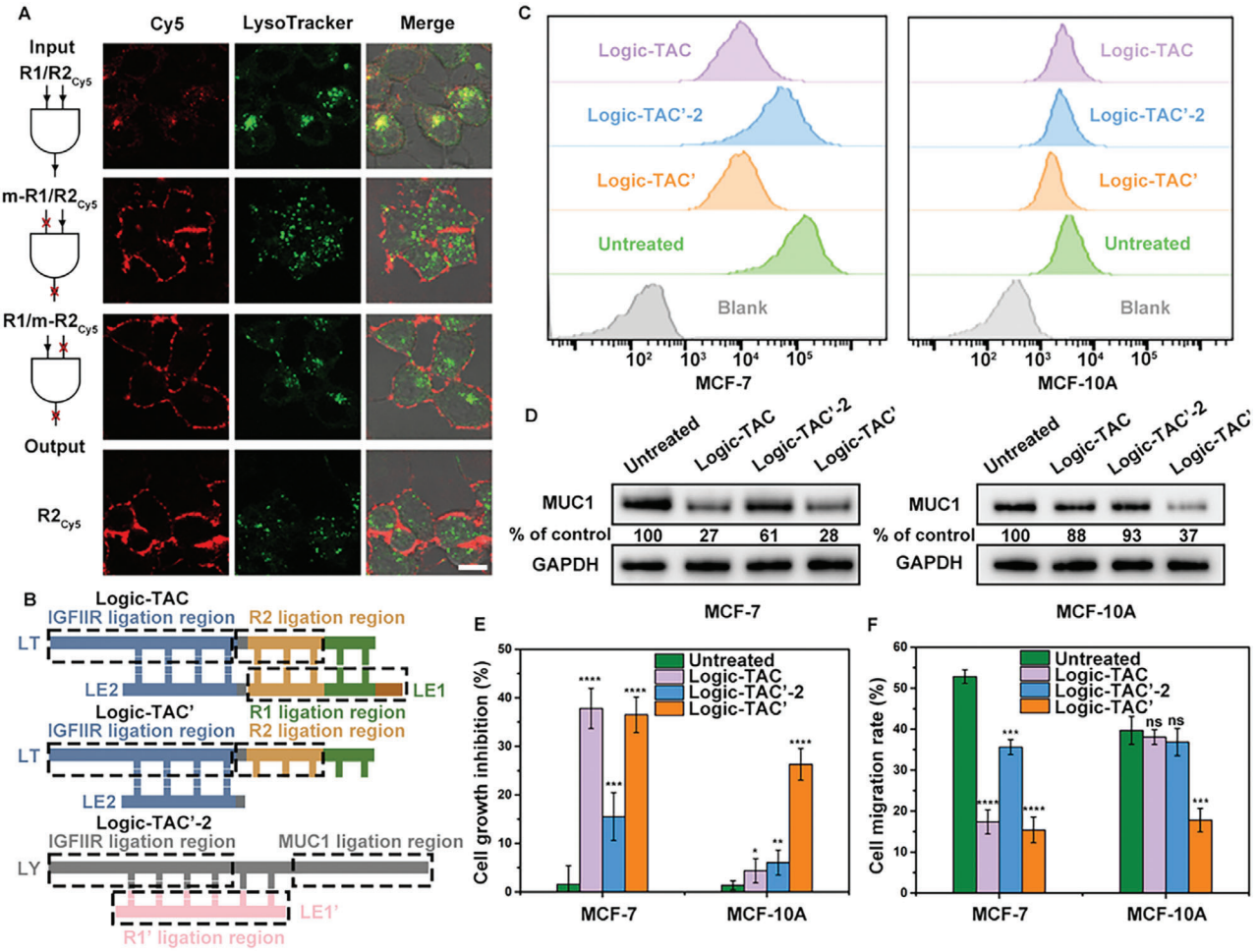

Figure 3. Cancer cell-selective MUC1 degradation. A) Confocal microscopic images of Logic-TAC incubated MCF-7 cells that pretreated with $R1/R2_{Cy5}$, m-$R1/R2_{Cy5}$, R1/m-$R2_{Cy5}$, and MCF-7 cells that only treated with $R2_{Cy5}$, followed by co-localization with LysoTracker Green. The scale bar is 15 μm. B) Schematic illustration of Logic-TAC, Logic-TAC', and Logic-TAC'-2. C) Flow cytometry analysis, D) immunoblot, E) quantification of cell growth inhibition and F) cell migration rate of MCF-7 cells or MCF-10A cells (Untreated) and MCF-7 cells and MCF-10A cells respectively treated with Logic-TAC, Logic-TAC', Logic-TAC'-2. The level of MUC1 expression for untreated MCF-7 cells or MCF-10A cells was set as the control in (D). The data error bars in (E) and (F) indicate means ± S.D. (n = 3). $^{*}p < 0.05$, $^{**}p < 0.01$, $^{***}p < 0.001$, and $^{****}p < 0.0001$ with two-tailed Student's t-test.

degradation for both MCF-7 cells and MCF-10A cells (Figure 3D). These results demonstrated similar tendency as flow cytometry results, indicating SECORE strategy could provide satisfactory POI degradation selectivity and efficiency. As verified by flow cytometry, SECORE strategies didn't affect EpCAM expression compared with untreated cells (Figure S17, Supporting Information), guaranteeing the safe application of SECORE strategy with little nonspecific protein degradation.

Cell proliferation and invasion were further studied by CCK-8 and wound healing assay. Logic-TAC treatment showed satisfactory discrimination of cancer cells and noncancerous cells for MUC1 degradation. 37.8% of cell growth inhibition and 18.7% of cell mobility were obtained for MCF-7 cells, while 4.3% of cell growth inhibition and 38.1% of cell mobility were obtained for MCF-10A cells (Figure 3E,F; Figures S18 and S19, Logic-TAC, Supporting Information). Logic-TAC' in absence of cancer cell selectivity demonstrated obvious nonspecific toxicity to MCF-10A cells with cell growth inhibition of 26.3% and cell mobility of 17.8% (Figure 3E,F; Figure S19, MCF-10A, Logic-TAC', Supporting Information). Logic-TAC'-2 with uncontrolled ligation orders to MUC1 and IGFIIR showed impaired MUC1 degradation efficiency for MCF-7 cells with 15.5% of cell growth inhibition and 35.6% of cell mobility (Figure 3E,F; Figure S18, MCF-7, Logic-TAC'-2, Supporting Information). Cellular functions of proliferation and invasion demonstrated similar tendencies as MUC1 expression levels corresponding to different LYTAC strategies, confirming the applicability of SECORE strategy for selective and efficient membrane protein degradation.

2.5. *In Vivo* Application of SECORE Strategy for Tumor Growth Inhibition

Phosphorothioate DNA strands were used to increase *in vivo* stability. The stability of Logic-TAC was tested in the 10% FBS, which showed similar migration distances for different incuba-

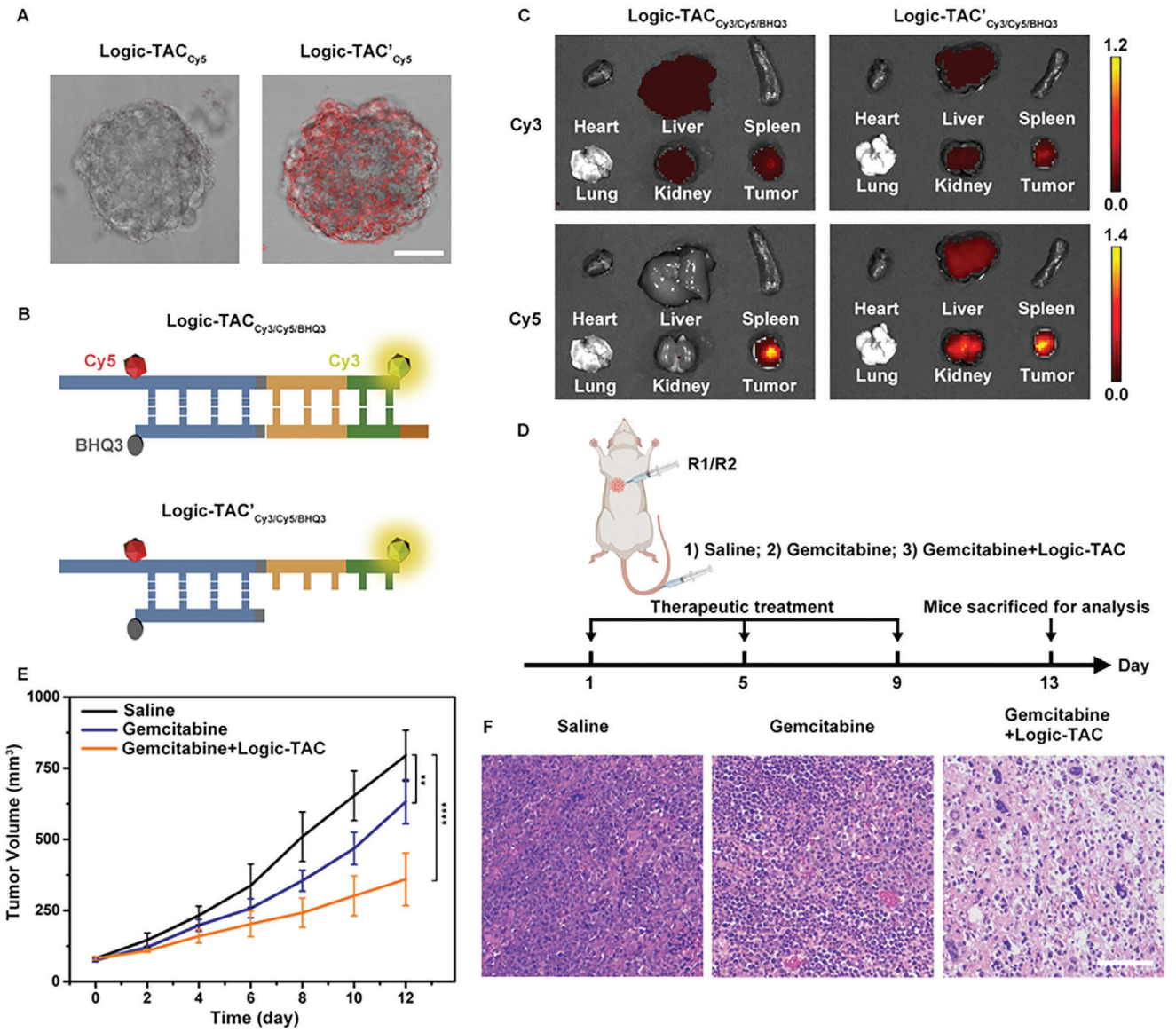

Figure 4. Activatable imaging and antitumor efficacy. A) 3D-stack images of MCF-10A multicellular spheroids treated with Logic-TAC$_{Cy5}$ and Logic-TAC'$_{Cy5}$. The scale bar is 50 μm. B) Schematic illustration of Logic-TAC$_{Cy3/Cy5/BHQ3}$ and Logic-TAC'$_{Cy3/Cy5/BHQ3}$. C) *Ex vivo* fluorescence imaging of organs and tumors harvested from mice treated with Logic-TAC$_{Cy3/Cy5/BHQ3}$ and Logic-TAC'$_{Cy3/Cy5/BHQ3}$ respectively. D) Schematic illustration of *in vivo* therapy protocol. E) Tumor growth curves and F) representative H&E staining images of tumor tissues from mice treated with saline, gemcitabine, mixture of gemcitabine+Logic-TAC (1 μM). The data error bars indicate means ± S.D. (n = 5). The scale bar is 100 μm. $^{**}p < 0.01$ and $^{****}p < 0.0001$ with two-tailed Student's t-test.

tion time up to 24 h (Figure S20A, Supporting Information). Logic-TAC$_{Cy5/BHQ3}$ also showed very low Cy5 fluorescence recovery during 24-h incubation (Figure S20B, Supporting Information), indicating its configuration stability. MCF-10A multicellular spheroid was established, pretreated with R1/R2, and incubated with Logic-TAC$_{Cy5}$ and Logic-TAC'$_{Cy5}$ respectively to verify the capability of SECORE strategy to protect normal tissue from nonspecific toxicity. Compared with Logic-TAC'$_{Cy5}$, Logic-TAC$_{Cy5}$ barely showed Cy5 fluorescence, indicating its little anchoring to MCF-10A due to its absence of EpCAM expression (**Figure 4A**; Figure S21, Supporting Information). This result indicated the minimal influence of SECORE strategy to noncancerous cells.

Mice bearing orthotopic MCF-7 tumors were chosen as the model. To study the pharmacokinetics of Logic-TAC, Logic-TAC$_{Cy5}$ was intravenously administrated into mice, and blood was collected at different time after the injection. The blood-circulation half-time was calculated as 11.6 min (Figure S22A, Supporting Information). Pretreatment with R1/R2 caught Logic-TAC$_{Cy5}$ from systeatic circulation to tumor position, and reached maximum accumulation at 1–2 h after administration (Figure S22B,C, Supporting Information). The close location of R1 and R2 guaranteed the efficient capture of active Logic-TAC' at tumor position with little leakage. Therefore, incubating Logic-TAC$_{Cy5/BHQ3}$ with R1/R2 pretreated mice barely showed

Cy5 fluorescence at other organs, indicating little diffusion of activated Logic-TAC' out of tumor position (Figure S23, Supporting Information). In the absence of R1/R2, there was no nonspecific activation of Logic-TAC$_{Cy5/BHQ3}$, which showed little Cy5 fluorescence recovery in organs (Figure S24, Supporting Information).

The *in vivo* cancer cell-selective activation of Logic-TAC was further monitored with Logic-TAC$_{Cy3/Cy5/BHQ3}$. Cy3 acted as "always on" dye to indicate organ distribution of Logic-TAC probe, while Cy5 located in proximity to BHQ3 to make a self-quenched structure, acted as "activatable" dye to indicate the activation of Logic-TAC probe (Figure 4B, Logic-TAC$_{Cy3/Cy5/BHQ3}$). Logic-TAC'$_{Cy3/Cy5/BHQ3}$ with exposed L1 region on LT was synthesized by hybridizing LT$_{Cy3/Cy5}$ with LE2$_{BHQ3}$ to demonstrate its nonspecific activation outside tumor position (Figure 4B, Logic-TAC'$_{Cy3/Cy5/BHQ3}$). Mice were pretreated with R1/R2 and intravenously administrated with Logic-TAC$_{Cy3/Cy5/BHQ3}$ and Logic-TAC'$_{Cy3/Cy5/BHQ3}$ respectively. Both Logic-TAC$_{Cy3/Cy5/BHQ3}$ and Logic-TAC'$_{Cy3/Cy5/BHQ3}$ were pretreated with R2 to mimic the *in vivo* nonspecific activation from noncancerous cell MUC1. Cy5 fluorescence was observed only at tumor grown position with little background at other organs for Logic-TAC$_{Cy3/Cy5/BHQ3}$ treated mice, while Logic-TAC'$_{Cy3/Cy5/BHQ3}$ treated mice showed Cy5 fluorescence both from tumor grown position and livers/kidneys (Figure S25B, Supporting Information). The *ex vivo* imaging of the harvested organs and tumors showed the consistent results. Though Cy3 fluorescence was observed in both tumors and livers/kidneys due to the distribution of DNA strands, Cy5 fluorescence, as indicator of LYTAC probe activation for MUC1 degradation, was observed for Logic-TAC$_{Cy3/Cy5/BHQ3}$ injected mice group with 85.7% of Cy5 fluorescence distribution at tumor grown position (Figure 4C; Figure S25A, Logic-TAC$_{Cy3/Cy5/BHQ3}$, Cy5, Supporting Information), but spread to other organs with only 14.2% of Cy5 fluorescence distribution at tumor grown position for Logic-TAC'$_{Cy3/Cy5/BHQ3}$ injected mice group (Figure 4C; Figure S25A, Logic-TAC'$_{Cy3/Cy5/BHQ3}$, Cy5, Supporting Information). These results guaranteed the successful *in vivo* application of SECORE strategy for cancer cell-selective POI degradation.

To evaluate the anticancer capability of SECORE strategy, breast cancer bearing mice were divided into three groups, pretreated by intratumoral injection of R1/R2, followed by intravenously administrated with 1) saline; 2) chemotherapeutic drug gemcitabine; 3) gemcitabine and Logic-TAC mixture every 4 days (Figure 4D). The mice group administrated with Logic-TAC and gemcitabine demonstrated the highest inhibition of tumor growth compared with saline treated group and merely chemotherapeutic treated group (Figure 4E; Figure S26, Supporting Information), indicating the efficient contribution of POI degradation to cancer therapy. Different concentration (1 and 2 μM) of Logic-TAC was administrated respectively, and demonstrated similar contribution to tumor growth suppression (Figure S27, Supporting Information). H&E staining analysis also showed the largest extent of cell apoptosis in tumor tissue for Logic-TAC and gemcitabine treated mice group (Figure 4F). There was no weight loss (Figures S28 and S29, Supporting Information) nor damage to major organs (Figure S30, Supporting Information) for all the mice groups, indicating the good biocompatibility of SECORE strategy.

3. Conclusion

A duplex DNA strand (Logic-TAC) was designed in this work, and achieved cancer cell MCF-7 selective MUC1 degradation *via* a cell membrane-guided logic gate calculation with no influence to MUC1 on normal cell MCF-10A. The ligation regions for POI MUC1 and IGFIIR were blocked in Logic-TAC by hybridizing with two complementary DNA strands, which deactivated Logic-TAC before it arrived at target tumor cells and avoided systematic toxicity to normal cells. To perform input 1 for DNA logic gate, EpCAM, as indicator protein to discriminate cancer cell MCF-7 with normal cell MCF-10A, reacted with Logic-TAC to expose its MUC1 ligation region. To perform input 2 for DNA logic gate, the above obtained "activated" Logic-TAC bound to membrane MUC1 and exposed IGFIIR ligation region. As output of DNA logic gate, MUC1 was coupled to IGFIIR and correspondingly degraded *via* lysosomal pathway. Nucleic acids-based LYTAC reagents provided precisely designed sequence, controllable configuration, more convenient preparation process with less cost. The as-presented cancer cell-selective Logic-TAC protein degradation strategy not only suppressed side effect to normal cells, but also improved degradation efficiency by avoiding invalid consumption of LYTAC reagent that do not bind to MUC1 wtih good *in vivo* therapeutic results. Considering the limited types of LTRs, developing lysosomal targeting strategies that don't rely on LTRs could be the direction for future research, which would fit LYTAC for cancer cell types that don't express LTRs. To make the as-presented strategy for future clinic applications, regulatory considerations include encapsulation and delivery process standardization and release process *in vivo* monitoring and evaluation.

Supporting Information

Supporting Information is available from the Wiley Online Library or from the author.

Acknowledgements

The authors gratefully acknowledge the National Natural Science Foundation of China (22022405, 22374073, 21974064, 22104063), Natural Science Foundation of Jiangsu Province for distinguished Young Scholars (BK20200010), State Key Laboratory of Analytical Chemistry for Life Science (5431ZZXM2204, 5431ZZXM2307), Natural Science Foundation of Jiangsu Province, China (SBK2021042488), Program B for Outstanding PhD Candidates of Nanjing University.

Conflict of Interest

The authors declare no conflict of interest.

Data Availability Statement

The data that support the findings of this study are available from the corresponding author upon reasonable request.

Keywords

cancer therapy, cell membrane engineering, DNA nanostructure, logic gate, membrane protein degradation

Received: November 4, 2023
Revised: February 18, 2024
Published online:

[1] J. N. Sachs, D. M. Engelman, *Annu. Rev. Biochem.* **2006**, *75*, 707.
[2] B. Liang, L. K. Tamm, *Nat. Struct. Mol. Biol.* **2016**, *23*, 468.
[3] A. Krogh, B. Larsson, G. von Heijne, E. L. Sonnhammer, *J. Mol. Biol.* **2001**, *305*, 567.
[4] M. P. Muller, T. Jiang, C. Sun, M. Lihan, S. Pant, P. Mahinthichaichan, A. Trifan, E. Tajkhorshid, *Chem. Rev.* **2019**, *119*, 6086.
[5] I. Levental, E. Lyman, *Nat. Rev. Mol. Cell Biol.* **2023**, *24*, 107.
[6] H. Yin, A. D. Flynn, *Annu. Rev. Biomed. Eng.* **2016**, *18*, 51.
[7] M. A. Yildirim, K. I. Goh, M. E. Cusick, A. L. Barabasi, M. Vidal, *Nat. Biotechnol.* **2007**, *25*, 1119.
[8] S. M. Banik, K. Pedram, S. Wisnovsky, G. Ahn, N. M. Riley, C. R. Bertozzi, *Nature* **2020**, *584*, 291.
[9] Y. Miao, Q. Gao, M. Mao, C. Zhang, L. Yang, Y. Yang, D. Han, *Angew. Chem., Int. Ed.* **2021**, *60*, 11267.
[10] Y. Liu, X. Qian, C. Ran, L. Li, T. Fu, D. Su, S. Xie, W. Tan, *ACS Nano* **2023**, *17*, 6150.
[11] S. B. Alabi, C. M. Crews, *J. Biol. Chem.* **2021**, *296*, 100647.
[12] Y. Ding, D. Xing, Y. Fei, B. Lu, *Chem. Soc. Rev.* **2022**, *51*, 8832.
[13] K. Hamada, T. Hashimoto, R. Iwashita, Y. Yamada, Y. Kikkawa, M. Nomizu, *Cell Rep. Phys. Sci.* **2023**, *4*, 101296.
[14] K. Moreau, M. Coen, A. X. Zhang, F. Pachl, M. P. Castaldi, G. Dahl, H. Boyd, C. Scott, P. Newham, *Br. J. Pharmacol.* **2020**, *177*, 1709.
[15] D. W. Kufe, *Cancer Biol. Ther.* **2009**, *8*, 1197.
[16] C. R. Bakshani, A. L. Morales-Garcia, M. Althaus, M. D. Wilcox, J. P. Pearson, J. C. Bythell, J. G. Burgess, *npj Biofilms Microbiomes* **2018**, *4*, 14.
[17] K. Raina, J. Lu, Y. Qian, M. Altieri, D. Gordon, A. M. K. Rossi, J. Wang, X. Chen, H. Dong, K. Siu, J. D. Winkler, A. P. Crew, C. M. Crews, K. G. Coleman, *Proc. Natl. Acad. Sci. USA* **2016**, *113*, 7124.
[18] K. An, X. Deng, H. Chi, Y. Zhang, Y. Li, M. Cheng, Z. Ni, Z. Yang, C. Wang, J. Chen, J. Bai, C. Ran, Y. Wei, J. Li, P. Zhang, F. Xu, W. Tan, *Angew. Chem., Int. Ed.* **2023**, *62*, e202306824.
[19] J. Liu, H. Chen, Y. Liu, Y. Shen, F. Meng, H. Ü. Kaniskan, J. Jin, W. Wei, *J. Am. Chem. Soc.* **2021**, *143*, 7380.
[20] C. Zhang, Z. Zeng, D. Cui, S. He, Y. Jiang, J. Li, J. Huang, K. Pu, *Nat. Commun.* **2021**, *12*, 2934.
[21] S. He, F. Gao, J. Ma, H. Ma, G. Dong, C. Sheng, *Angew. Chem., Int. Ed.* **2021**, *60*, 23299.
[22] H.-J. Liu, W. Chen, G. Wu, J. Zhou, C. Liu, Z. Tang, X. Huang, J. Gao, Y. Xiao, N. Kong, N. Joshi, Y. Cao, R. Abdi, W. Tao, *Adv. Sci.* **2023**, *10*, 2207439.
[23] M. A. Maneiro, N. Forte, M. M. Shchepinova, C. S. Kounde, V. Chudasama, J. R. Baker, E. W. Tate, *ACS Chem. Biol.* **2020**, *15*, 1306.
[24] C. Zhang, S. He, Z. Zeng, P. Cheng, K. Pu, *Angew. Chem., Int. Ed.* **2022**, *61*, e202114957.
[25] C. Liang, Q. Zheng, T. Luo, W. Cai, L. Mao, M. Wang, *CCS Chem* **2022**, *4*, 3809.
[26] J. Paulk, *Nat. Chem. Biol.* **2021**, *17*, 931.
[27] D. F. Caianiello, M. Zhang, J. D. Ray, R. A. Howell, J. C. Swartzel, E. M. J. Branham, E. Chirkin, V. R. Sabbasani, A. Z. Gong, D. M. McDonald, V. Muthusamy, D. A. Spiegel, *Nat. Chem. Biol.* **2021**, *17*, 947.
[28] K. Pedram, D. J. Shon, G. S. Tender, N. R. Mantuano, J. J. Northey, K. J. Metcalf, S. P. Wisnovsky, N. M. Riley, G. C. Forcina, S. A. Malaker, A. Kuo, B. M. George, C. L. Miller, K. M. Casey, J. G. Vilches-Moure, M. J. Ferracane, V. M. Weaver, H. Läubli, C. R. Bertozzi, *Nat. Biotechnol.* **2023**, https://doi.org/10.1038/s41587023018406.
[29] W. Chen, Z. Zhang, S. Zhang, P. Zhu, J. K.-S. Ko, K. K.-L. Yung, *Int. J. Mol. Sci.* **2021**, *22*, 6567.
[30] B. Ballester, J. Milara, J. Cortijo, *Eur. Respir. Rev.* **2021**, *30*, 200149.
[31] T. Gao, B. Wang, L. Shi, X. Zhu, Y. Xiang, J. Anzai, G. Li, *Anal. Chem.* **2017**, *89*, 10776.
[32] Z. Chen, H. Liu, A. Jain, L. Zhang, C. Liu, K. Cheng, *Theranostics* **2017**, *7*, 2982.